

Initial Steps of the Photodissociation of the CO Ligated Heme Group

Barry D. Dunietz,[†] Andreas Dreuw,[†] and Martin Head-Gordon*

Department of Chemistry, University of California at Berkeley, and Chemical Sciences Division, Lawrence Berkeley National Laboratory, Berkeley, California 94720

Received: December 21, 2002; In Final Form: March 31, 2003

Upon irradiation of CO ligated hemoglobin or myoglobin with a laser pulse of 570 nm (2.17 eV), the proteins are electronically excited into the Q states and undergo dissociation of the CO ligand within 50 fs. Because the Q state is well-known to correspond to a π – π^* transition localized at the iron porphyrin (heme) group, this should not greatly affect the binding of the CO ligand. It is shown by means of time-dependent density functional theory that, in fact, the Q states decay into the 5 A'' and 3 A' singlet excited states. The latter states are repulsive along the Fe–CO stretch coordinate and, consequently, lead to the dissociation of the heme–CO bond. The nature of the repulsive states is analyzed with attachment/detachment density plots. At the equilibrium geometry of heme–CO, they can be understood as an excitation from a π -back-bonding orbital into an anti-back-bonding orbital which nicely explains their repulsive nature. However, at a separation distance of 2.5 Å, the state has charge-transfer character from the iron to the nitrogens of the porphyrin ring as well as the CO and imidazole ligand. This is in accord with a previous experimental assignment of the first intermediate of the photodissociation process to be a charge-transfer state.

Introduction

Iron porphyrin, which is usually referred to as heme group, is found as prosthetic group at the core of some enzymes of biological significance. These enzymes include for example cytochrome *c*, peroxidase, hemoglobin (Hb), and myoglobin (Mb). In cytochrome *c* and peroxidase, the heme group participates in the catalysis of important redox reactions, whereas in Hb and Mb, the heme group is responsible for reversibly binding oxygen. The structure of the heme group in the hemoproteins Mb and Hb is very similar, although Hb contains four heme groups and is considered an allosteric tetrameric protein, whereas Mb has only one heme group. The only covalent link of the heme group to the embedding protein is through a histidine iron bond. Consequently, the absorbed ligands, e.g., O₂ and CO, are attached to the iron from the opposite side of the iron–porphyrin system. Naturally, Hb is found in red blood cells and is responsible for oxygen transport and Mb is found in muscle tissues and is used to store oxygen.

Because the functionality of the hemoproteins is based on their ability to reversibly bind O₂, the ligation of Hb and Mb by small molecules such as O₂, NO, and CO has been the focus of extensive research.^{2,7,11–13} The importance of the oxygen ligand is obvious, and NO and CO binding is important with respect to NO and CO poisoning and other functionalities^{7,14} (see for example ref 15 for a recent review of the functionality of Mb with respect to the interaction with NO radicals). Another important aspect of CO binding is that MbCO is spectroscopically easier to observe than MbO₂. Consequently, most experiments addressing the binding kinetics of heme proteins use CO ligated Mb or Hb. The preference for MbCO arises from the presence of a very fast rebinding component and of geminate rebinding in MbO₂ and the strong IR bands of CO in heme proteins which are superb spectroscopic markers.

Because the heme–CO system is characterized by an intense and typical absorption spectrum, it is generally a well suited model system for investigations of photodissociation initiated relaxation processes.^{1,5} Indeed, the photodissociation of the heme–ligand bond is experimentally often used as initial step in studies of protein dynamics.^{3,4,6,16,17} It is a convenient way to generate intermediates which can undergo nonradiative decay including electron transfer reactions. The mechanisms of such electron transfer processes have been widely investigated (see ref 18 for an overview and ref 19 for a recent review of the experimental methodology).

In the past few years, the use of quantum chemical methods has been extended to study complex systems. Biological systems serve as an obvious and important example for this trend. The focus of this research has mainly been the investigation of the mechanisms by which enzymes function, which involves mapping the ground state of the system at the various steps of the catalytic cycle. Thus, less attention has been paid to excited states studies, although, some excited states play important roles in biological processes, e.g., vision and photosynthesis.

Much attention has been paid experimentally and computationally to the orientation of which CO is bonded to the heme iron atom. Early X-ray structure studies^{22–25} indicated a tilted orientation of CO. These studies led to the belief that the orientation of the CO ligand is crucial for the mechanism by which the heme containing proteins are able to suppress the binding energy of CO relative to O₂ as opposed to binding of these ligands to the free heme.²¹ However, other spectroscopical experiments (IR Raman spectroscopy, solid NMR, and Mössbauer studies) suggest an almost up right orientation.^{13,26–28} Recent refined X-ray studies have confirmed these spectroscopical observations of a nearly linear CO binding geometry,^{9,10} and it was demonstrated⁸ that the early indication for the tilted orientation was an artifact of the X-ray data refinement. Computational studies have demonstrated that the energetic penalty for bending and tilting the CO is small²⁰ However,

* To whom correspondence to be addressed: E-mail: mhg@bastille.cchem.berkeley.edu.

[†] Both authors contributed equally.

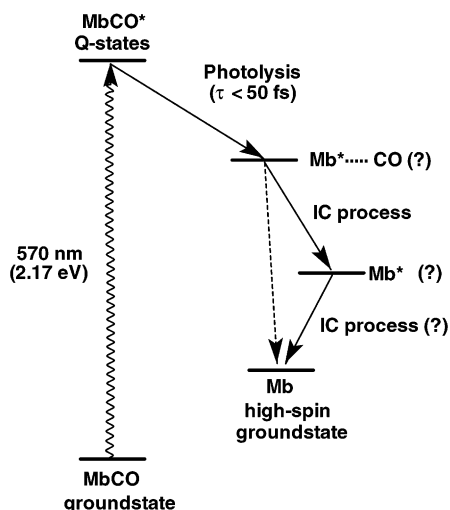


Figure 1. Sketch of the energy level scheme for the photodissociation process of CO ligated Mb.

although this system has been widely studied the properties of its excited states remain elusive.

In this work, we focus on the photodissociation of CO ligated heme and provide insight into the mechanism by which excited states participate in the process. Proteins with a CO ligated heme undergo dissociation of the Fe–CO bond²⁹ upon pulsed illumination at 570 nm (2.18 eV). This reaction is the most investigated of its kind.³⁰ It is a complicated process which involves several steps, the energy levels of which are sketched in Figure 1. In the figure, experimental estimates for the time scales of the different transitions are provided. The first step in this process is a vertical excitation to the lowest excited state (the Q band). This is the well-known π – π^* transition in systems involving porphyrins. The photoexcitation step is followed by fast dissociation, in about 50 fs, to an intermediate excited state.^{31–33} The short time scale of this step excludes the possibility of a change in the spin state of the system. The similarities of the excited states lifetimes and absorption maxima in the spectra of both ligated and unligated forms indicate that the first fast step already results in the dissociation of the ligand.^{32,33}

The available experimental data also shows that the iron moves out of the plane of the porphyrin ring almost instantly upon photodissociation.^{16,33} Although the iron atom is located within the plane of the porphyrin ring in the ligated form of the heme, it is about 0.3 Å out of the plane in the unligated species. This iron motion is probably related to the change in the spin state, where the iron switches from the low-spin configuration in the ligated species to the high-spin state of the unligated form. Experimentally, the iron motion is observed through the frequency shift of the Fe–His mode in the resonance Raman spectrum.^{16,33} This mode assignment is confirmed by the absence of the mode shift in the spectra of the ligated form and by X-ray studies.⁹ The experiments show that the iron motion is very fast and happens within about 300 fs. However, it is still unclear whether the iron movement follows the dissociation to yield another intermediate or the first intermediate has already the iron placed out of the heme plane.

In addition, experimental data^{16,33} indicates that the fast heme dissociation step is followed by several steps including gradual structural changes and probably more than one excited intermediate state.^{32,33} This is depicted in Figure 1, where the path of relaxation to the ground state of unligated Hb proceeds through several intersystem crossing (IC) steps. Alternatively,

a different interpretation of the Raman spectra has suggested that the relaxation process following the photodissociation is dominated by populating the vibrational modes of the ground electronic state.¹⁶

As discussed above, the data accumulated on the photodissociation process of heme–CO suggests that the fast first step leads already to a dissociated intermediate. Different models for describing the relevant excited states have been suggested.^{34,35} However, the identification of the first excited intermediate state as a charge transfer (CT) state has been given only recently by Franzen et al.³³ Although this was suggested earlier by Vogler and Kunkley,³⁶ it was not backed up by experimental data. The assignment of the first excited intermediate state to a CT state by Franzen et al. has suggested a mechanism for the photolysis which was not considered before: the removal of one bonding electron from an iron–CO ($d_{\text{Fe}}-\pi_{\text{CO}}^*$) orbital resulting in reduced back-bonding of the ligands to the iron. In addition, the possibility of an involvement of a high spin state in the primary photodissociation step has been ruled out.³³

Here, we characterize the relevant excited states for the photodissociation step of CO ligated heme by means of ab initio quantum chemistry. The paper is organized as follows. In the next section, we describe the computational methods and models used in our calculations. Thereafter, we present our results, where we first focus on the ground-state equilibrium structure of the CO ligated heme and the excited-state properties at that geometry. Then, we investigate the potential surface of the excited states with respect to the CO dissociation coordinate and analyze the nature of the excited states relevant for the dissociation process. Finally, we conclude with a brief summary and outlook on possible future work.

Computational Details

The quantum chemical description of the excited states of a large molecular system like Mb or Hb is only possible if a suitable model is chosen and its validity is checked against available experimental data. In our study of the excited states of CO ligated Mb and Hb, we exclude the protein backbone from the quantum chemical calculation because the protein has minor influence on the excited states which are localized at the reaction center. Furthermore, the side chains of the original reaction center of Hb and Mb, the heme group, are removed for the same reason. The role of the side chains is primarily to keep the heme group in place by van der Waals interactions and hydrogen bonds with the protein. Finally, we replaced the histidine residue, which is the only covalent link of the iron–porphyrin ring to the protein backbone, by an imidazole ring. This substitution is justified because the electronic characteristics of the imidazole ring resemble those of the histidine residue. Following this procedure, we obtained the model complex displayed in Figure 2. Although the structural approximations seem to be rather limiting, the model complex turned out to be suitable for the calculation of the electronic excitation spectrum of Mb. Using this model complex, Tokita and Nakatsuji could already recover the relevant features of the excitation spectra of CO ligated Mb using their symmetry adapted cluster configuration interaction (SAC–CI) approach,³⁷ whereas McMahon et al. presented a ground state study using a microscopic model of carbon monoxide binding to myoglobin.³⁸

Our quantum chemical study comprises the geometry optimization of the model complex and the calculation of the vertical excitation spectra of the system along the iron–carbon stretch coordinate. The geometry optimization of the model complex

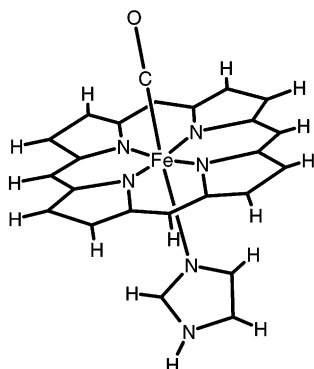


Figure 2. Model complex for CO ligated heme that has been used within our calculations.

TABLE 1: Comparison of Selected Geometrical Parameters Optimized at the Level of DFT/BLYP/LanL2DZ and DFT/B3LYP/LanL2DZ with Experimental Values^a

	BLYP	B3LYP	expt. ^{39,40}
$r(\text{Fe}-\text{CO})$	1.81	1.80	1.73–1.93
$r(\text{Fe}-\text{N}_\text{P})$	2.01	2.03	1.98–2.06
$r(\text{Fe}-\text{N}_\text{I})$	1.98	2.04	2.06–2.20
$r(\text{C}-\text{O})$	1.21	1.16	1.07–1.12

^a The use of different functionals has only negligible influence on the geometry.

was carried out at the level of density functional theory (DFT) using various functionals and basis sets. We used the local Slater–Vosko–Wilk–Nusair (SVWN), the gradient-corrected Becke–Lee–Yang–Parr (BLYP), as well as the widely used hybrid B3LYP functional in combination with different basis sets with or without effective core potentials on the central iron atom. The obtained equilibrium structure is more or less independent of the functional/basis set combination, and the structural parameters are in very good agreement with available experimental data on human CO ligated Hb³⁹ and Mb.⁴⁰ In Table 1, selected geometrical parameters calculated with the BLYP and B3LYP functional and the 6-31G basis set as well as the Los Alamos effective core potential at the iron atom are compared with the corresponding experimental values.^{39,40} The parameters vary only slightly between the BLYP and the B3LYP functional, but the latter is still a little bit closer to the experimental values. The same is true for the SVWN functional (results not provided here). Therefore, we use the B3LYP/LANL2DZ optimized geometry within all calculations.

In contrast to the geometry optimization, the different functionals perform very differently when the excitation energies were calculated with the time-dependent DFT (TDDFT) method. The calculated electronic excitation spectra depend very strongly on the choice of the functional/basis set combination. For this reason, we performed a detailed study of the dependence of the excitation energies on the functional and basis set. We compared the calculated values with the known experimental data for the Q and B bands of CO ligated Mb,⁴¹ the SAC–CI calculations by Tokita and Nakatsuji,³⁷ and the configuration interaction singles (CIS) values (Table 2). The values given in Table 2 are calculated at the B3LYP optimized geometry. The use of the BLYP or SVWN optimized geometry for the excited state calculations employing TDDFT with the BLYP or SVWN functional, respectively, has only negligible influence on the excitation energies.

The SVWN and BLYP functionals give values for the B band that are very close to the experimental value, whereas the Q band is underestimated by up to 0.8 eV. These functionals seem

TABLE 2: Dependence of the Energies of the Q and B Band of CO Ligated Heme on the Exchange-Correlation Functional and the Basis Set^a

excited state:	Q_1	Q_2	B_1	B_2
SVWN				
LAN2DZ	1.5150	1.5369	3.0093	3.0204
6-31G	1.3338	1.3568	2.8994	2.9215
6-31G*	1.3908	1.4128	2.9038	2.9250
BLYP				
LAN2DZ	1.8226	1.8428	3.0493	3.0559
6-31G	1.5057	1.5271	2.9292	2.9524
6-31G*	1.5727	1.5933	2.9266	2.9434
B3LYP				
LAN2DZ	2.4039	2.4177	3.3458	3.3591
6-31G	2.3354	2.3961	3.6902	3.6976
6-31G*	2.4027	2.4127	3.3140	3.3250
CIS				
LAN2DZ	2.5620	2.5653	4.4428	4.4820
6-31G*	2.4898	2.4907	4.4231	4.4629
SAC/CI³⁷				
	1.84	1.94	3.36	3.41
expt.⁴¹				
	2.18	2.30	2.96	3.16

^a The energies were calculated using TDDFT at the B3LYP optimized geometry of the model complex (Figure 2).

to treat the electronically excited states corresponding to the Q and B bands in an unbalanced fashion. Only the B3LYP functional shows a consistent error for both bands and overestimates them by about 0.2–0.3 eV. Furthermore, the calculated excitation energies depend only slightly on the choice of the basis set. Neither the use of an effective core potential nor the addition of polarization functions has a significant influence on the results for the excitation energies. Because the B3LYP functional provides the most balanced treatment of the excited states of our system, we have chosen it in combination with the LANL2DZ (6-31G basis set in combination with the Los Alamos effective core potential⁴²) basis set as our standard for this study.

A short glance at the other methods shows that CIS overestimates the excitation energies drastically, as expected, and that the SAC–CI approach inconsistently treats the Q and B bands. Although the first band is underestimated by 0.3–0.4 eV, the latter is overestimated by the same error. Unfortunately, the use of more sophisticated wave function based methods is prohibitive for the time being due to the large size of the system.

Usually, the nature of excited states is analyzed by looking at the molecular orbitals of the ground-state involved in the excitation. This can be very tedious, when many molecular orbitals with different coefficients have to be considered. In this work, we use attachment/detachment density plots to interpret the excited states.⁴³ For this objective, the difference density matrix is diagonalized and decomposed in its negative and positive semidefinite parts. The negative part is called the detachment density matrix, because this part corresponds to the ground state density which is removed during the excitation. The positive part is the attachment density which is added upon excitation. In other words, the detachment density is that part of the ground state density that is replaced by the attachment density upon excitation. Consequently, the attachment/detachment density plots uniquely define the nature of the transition.

All calculations reported here were performed within the QChem package of programs.⁴⁴

Results and Discussion

The geometry optimization of the C_s symmetric model complex (Figure 2) at the theoretical level of standard ground-

TABLE 3: Assignment of the 18 Energetically Lowest States of CO Ligated Heme^a

state	nature	energy (eV)	strength	expt.
1 A'	$\pi \rightarrow \pi^*$	2.4039	2.7×10^{-3}	2.18 Q _x
1 A''	$\pi \rightarrow \pi^*$	2.4177	1.1×10^{-3}	2.30 Q _y
2 A''	$d_{Fe} \rightarrow \sigma^*(Fe-N)$	2.5338	$<1 \times 10^{-4}$	
3 A''	$(\pi, (d_{Fe} - \pi^*_{CO})) \rightarrow \pi^*$	2.7014	$<1 \times 10^{-4}$	
2 A'	$(\pi, (d_{Fe} - \pi^*_{CO})) \rightarrow \pi^*$	2.7246	$<1 \times 10^{-4}$	
4 A''	$(\pi, (d_{Fe} - \pi^*_{CO})) \rightarrow \pi^*$	2.8046	$<1 \times 10^{-4}$	
5 A''	$(\pi, (d_{Fe} - \pi^*_{CO})) \rightarrow (d_{Fe}, \pi^*_{CO})^*$	2.8684	2.5×10^{-3}	
3 A'	$(\pi, (d_{Fe} - \pi^*_{CO})) \rightarrow (d_{Fe}, \pi^*_{CO})^*$	2.8829	1.6×10^{-3}	
4 A'	$d_{Fe} \rightarrow \pi^*$	2.9673	2.9×10^{-3}	
6 A''	$d_{Fe} \rightarrow \pi^*$	2.9812	1.9×10^{-3}	
5 A'	$(\pi, (d_{Fe} - \pi^*_{CO})) \rightarrow \pi^*$	3.1186	3×10^{-4}	
6 A''	$\pi - \pi^*$	3.3458	0.5734	2.96 B _x
7 A''	$\pi - \pi^*$	3.3591	0.6207	3.16 B _y
7 A'	$d_{Fe} \rightarrow \pi^*_{lm}, \pi^*_{CO}$	3.5269	1×10^{-4}	
8 A''	$(\pi, (d_{Fe} - \pi^*_{CO})) \rightarrow \pi^*_{CO}, \pi^*_{lm}$	3.7473	8×10^{-4}	
8 A'	$(\pi, (d_{Fe} - \pi^*_{CO})) \rightarrow \pi^*_{CO}, \pi^*_{lm}$	3.7678	1×10^{-4}	
9 A'	$\pi - \pi^*$	3.8783	1.8×10^{-2}	3.60 N
9 A''	$\pi - \pi^*$	3.9046	1.9×10^{-2}	

^a The energies of the excited states are given together with their oscillator strength and the known experimental values. Furthermore, the nature of the states is analyzed. Orbitals without subscript refer to porphyrin ring orbitals, whereas d_{Fe} stands for iron d orbitals. Note that $(d_{Fe} - \pi^*_{CO})$ corresponds to the back-bonding combination of an iron d and the CO π^* orbital and $(d_{Fe} - \pi^*_{CO})^*$ for their anti-bonding combination.

state density functional theory employing the B3LYP functional and the LanL2DZ basis set yielded a heme geometry (Table 1) which is very similar to the experimental structure of heme in Mb or Hb.^{39,40} The obtained geometry has been confirmed to be a minimum on the potential energy surface by an analysis of the harmonic frequencies, which all have real values. Most importantly, the distance of the Fe–CO bond is found to be 1.8 Å in a strictly linear orientation. Today it is well established that the CO group is linear in an unperturbed heme–CO complex^{9,10} (see also the Introduction). Furthermore, the equilibrium bond length of the Fe–CO bond is in excellent agreement with the experimentally determined values of 1.73–1.93 Å.^{39,40} The geometry optimization of the singlet ground state of the model complex also showed that the iron atom is located strictly within the plane of the porphyrin ring. This is attributed to the low-spin state of the iron,⁴⁵ and it is well-known that in the high-spin ground state of unligated heme the iron is placed about 0.1–0.3 Å above the porphyrin ring.^{16,46}

Calculation of the 18 lowest excited states of CO ligated heme at the optimized ground-state equilibrium geometry with the TDDFT method employing the B3LYP functional and the LanL2DZ basis set yielded the excitation energies and oscillator strengths listed in Table 3. In analogy to Tokita and Nakatsuji,³⁷ we find the two lowest states (1 A' and 1 A'') at an energy of 2.4039 and 2.4177 eV to be pure $\pi - \pi^*$ transitions and to correspond to the experimentally known Q_x and Q_y excitation states of the system, respectively. This is in good agreement with the experimental values of 2.18 and 2.30 eV.⁴¹ However, our assignment of the energetically higher excited states differs from the previous assignment. Most of the states are excitations involving the π orbital of the porphyrin ring as well as a binding combination of an iron d orbital with the π^*_{CO} orbital into various different virtual orbitals or combinations of them. In Table 3, a detailed description of the nature of the 18 lowest excited states is provided. Note that our calculated excitation energies for the B_x (6 A') and B_y (7 A'') as well as N band (9 A' and 9 A'') are also in good agreement with the ex-

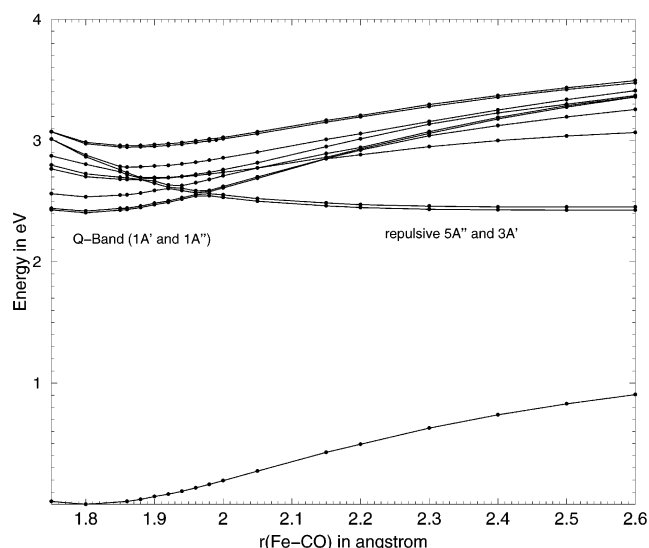


Figure 3. Potential energy curves of the ground state and singlet excited states of heme–CO along the Fe–CO dissociation coordinate calculated with TDDFT/B3LYP/LanL2DZ. The curves have been obtained without relaxation of other geometrical parameters. The lowest curves corresponds to the ground state of the system. The zero-point of the energy scale is set to the ground-state energy at its equilibrium geometry.

perimental values. The smaller energy splittings of the quasidegenerate Q, B, and N bands predicted by the calculation are probably due to the neglect of the embedding protein and/or solvent in our model.

To identify the relevant excited states for the photodissociation of the Fe–CO bond, we studied the excited states of heme–CO along the Fe–CO bond stretch coordinate. We successively increased the Fe–CO bond length from 1.75 to 2.6 Å and calculated the vertical excitation energy for each point using TDDFT/B3LYP/LanL2DZ without relaxing other geometrical parameters. In Figure 3, the obtained potential energy surfaces (PES) of the 18 energetically lowest excited states are presented along the Fe–CO dissociation coordinate. Our approach is justified because the initial photodissociation step is very fast and happens on a time scale of only 50 fs. Consequently, a redistribution of the internal vibrational energy and a full relaxation of the excited state geometry is not likely to occur in the given process. However, we have optimized the ground state geometry previously and did not observe any significant difference of the calculated excited-state surfaces along the Fe–CO stretch coordinate.⁴⁷ This leads us to conclude that geometry relaxation does not play a significant role for the investigated process, and we expect that the underlying physical picture will not change when the true minimum pathway is calculated, which is a desirable future refinement.

The calculated PESs provide much insight into the photodissociation process of heme–CO. Starting at the ground-state equilibrium structure, the system is excited into the Q band by a laser pulse of 2.17 eV. According to our results, the Q states are not repulsive along the Fe–CO dissociation coordinate but cross repulsive states at an Fe–CO separation of about 2 Å. The latter states are the only states that have a strong repulsive character. Consequently, the repulsive states, which are identified as 5 A'' and 3 A' at the equilibrium geometry, are the relevant excited singlet states that dissociate. The barrier that must be crossed for this decay is about 0.2 eV, which probably is an upper bound because we did not relax the geometry of the excited state. The energy to surmount this barrier is likely

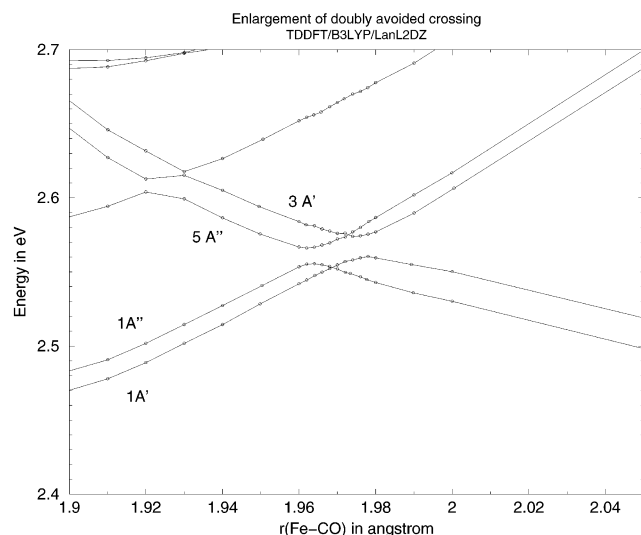


Figure 4. Enlarged part of the potential energy curves in the vicinity of the "crossing" of the Q states ($1 A'$ and $1 A''$) and the repulsive states ($5 A''$ and $3 A'$) at the equilibrium geometry. The nature of the "crossing" is shown to be a double avoided crossing along the unrelaxed Fe–CO stretch coordinate.

to be supplied simply by the associated vibrational mode and the vibrational excitation coinciding with the electronic excitation.

Calculation of the ground and singlet excited states of the unligated heme model using the same level of calculation shows that the excited states obtained from the simulation of the dissociation process converge to the states of the unligated species. Thus, the photodissociation process of the heme–CO complex is well described with our theoretical approach. Furthermore, it is evident from Figure 3 that at 2.5 Å the dissociation can be seen as complete, because further dissociation has no influence on the energy of the repulsive states. Once a CO separation of 2.5 Å is reached, complete dissociation follows.

Coming back to the photodissociation process, the relevant states for the dissociation process are the lowest excited states at both the ground-state equilibrium region and the dissociated region of the Fe–CO stretch coordinate. A first glance at Figure 3 suggests that the states $5 A''$ and $3 A'$ at the ground state equilibrium geometry cross through all other energetically lower lying states to become the lowest excited states at about 2 Å Fe–CO bond length. However, a careful examination of the different crossings reveals a more complex picture. In Figure 4, an enlarged projection of the "crossing" of the Q states ($1 A'$ and $1 A''$) and the repulsive $5 A''$ and $3 A'$ is provided. From this figure, it is obvious that these states do not cross along the defined CO stretch coordinate without geometry relaxation but that a doubly avoided crossing appears. Similar avoided crossings can be observed at the other energy crossings as well.

Let us now analyze the nature of the excited states $5 A''$ and $3 A'$, which are the relevant states for the photodissociation of the Fe–CO bond. In a previous communication,⁴⁷ we have seen that the excitations involve the linear combination of several molecular orbitals and have therefore used attachment/detachment density plots⁴³ to analyze the nature of these states. As an example, the attachment/detachment density plots of the $3 A'$ state is shown in Figure 5. The detachment density shown on the left-hand side of the figure is the part of the ground-state density which is replaced by the attachment density shown on the right-hand side. The rest of the ground-state density that

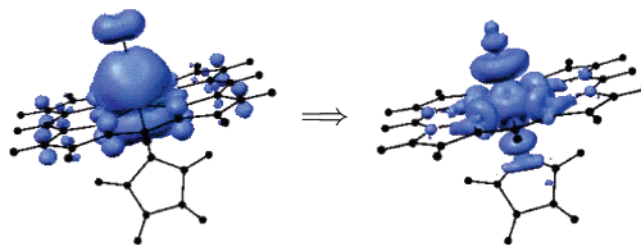


Figure 5. Attachment/detachment density plots of the repulsive state $3 A'$ at the ground-state equilibrium geometry of the model complex.

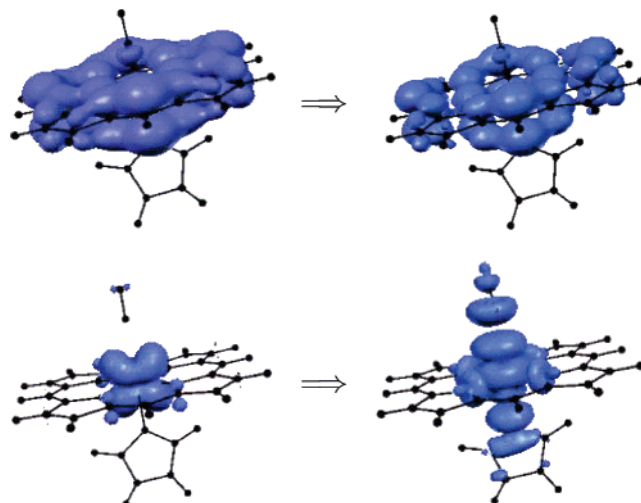


Figure 6. Attachment/detachment density plots of the energetically lowest excited state at the ground-state equilibrium geometry, the Q_y state (upper panel), and the lowest one at 2.5 Å Fe–CO separation, which is a repulsive state (lower panel).

remains unchanged during the excitation is not shown in the diagram. The isosurfaces shown are calculated for a 90% density enclosure. The density plot of the $5 A''$ state is essentially identical to the one of the $3 A'$ state (Figure 5), but the density is rotated by 90° around the Fe–CO axis.

Comparison of the detachment and attachment densities nicely explains the repulsive character of the $5 A''$ and $3 A'$ states. The detachment density is clearly dominated by a bonding iron–carbon interaction, whereas the attachment density has clearly antibonding character, which is seen as a node along the Fe–C bond. The bonding interaction between the iron atom and the CO ligand in the detachment density can be understood in chemical terms as back-bonding from an iron d orbital into the π^* orbital of CO. The antibonding interaction in the attachment densities corresponds to the antibonding combination of these orbitals (anti-back-bonding).

However, the $5 A''$ and $3 A'$ states are energetically never reached during the photodissociation process at the equilibrium geometry, but instead, the Q states can decay nonradiatively into these states by crossing the above-mentioned energy barrier. Consequently, one has to analyze the Q states and the repulsive states before and after the barrier, respectively, to get physical insight into the photodissociation process. Figure 6 provides the attachment/detachment density plots of these states. In the upper panel, the attachment/detachment density plots for the Q_y ($1 A'$) state are given, and one can easily see that they correspond to the expected π – π^* transition typical for porphyrin systems. The attachment/detachment density plots for the quasidegenerate Q_x ($1 A''$) state have the same appearance. In the lower panel, the corresponding density plots for the $1 A'$ state at large separation (i.e., the repulsive state) are shown at an Fe–CO distance of 2.5 Å. Here, it becomes clear that these

states correspond to the repulsive states identified above as states 5 A'' and 3 A' at the equilibrium region (see Figure 5). Consequently, the lowest excited states change their character from the π - π^* transition to the repulsive states when the barrier is crossed at about 2 Å Fe-CO separation. Further decay of the excited heme is thus expected to occur starting at these repulsive low lying excited states.

Comparison of the attachment/detachment density plots of the 3 A' state at the ground-state equilibrium geometry (Figure 5) with the ones obtained at 2.5 Å Fe-CO bond distance (lower panel of Figure 6) shows that the character of this state changes slightly along the Fe-CO stretch coordinate. As mentioned above, the 3 A' and 5 A'' states are dominated by an excitation of an electron from an Fe-CO back-bonding orbital into a anti-back-bonding orbital giving rise to the repulsive character of these states. At larger separations, where the bond is already broken, the states get more metal to porphyrin ring charge-transfer character. The attachment/detachment density plots of the repulsive 1 A' state (Figure 6) clearly indicate that charge is transferred from an iron d orbital to the CO and imadizole ligands as well as the nitrogens of the porphyrin ring. This agrees well with the experimental assignment of the first intermediate to a be a charge transfer state by Franzen et al.³³ Franzen suggested that the intermediate should possess iron-to-porphyrin ring charge transfer character because the spectrum of this state resembles the spectrum of the unligated anion. Indeed, the LUMO of the neutral unligated singlet heme model complex has exactly the same appearance as the attachment density of the repulsive 1 A' state at 2.5 Å Fe-CO separation.

The calculated PESs (Figure 3) do not exhibit the typical form which is expected for such fast reaction. Usually, a steep slope of the excited PES is found along the reaction coordinate in ultrafast photodissociation reactions, which provides an initial momentum for the wave packet to move on the excited PES. Specifically, the slopes of the ground and the Q states at the equilibrium geometry are similar. In addition, a small energy barrier must be crossed in order for the dissociation to occur. There are several possible explanations for this dilemma. First, the moderate slope might be a consequence of the restrictions inherent in the model. Probably, geometry relaxations of the Q states will result in steeper slopes along the reaction coordinate. In addition, this may also lead to further decrease of the already small energy barrier. Second, the crossing of the repulsive states with the Q band occurs at relatively short stretches (only 0.2 Å stretch). This suggests that upon excitation part of the vibrational wave packet on the excited PES is already beyond the energy barrier. Consequently, the excited wave packet has inherent dissociative character. Alternatively, because the crossing occurs close to the ground-state geometry, it is possible that, in the diabatic picture, the repulsive states are coupled to the Q state even at equilibrium. As a consequence, the PESs of the Q states have already repulsive character at low stretches. Finally, the frequency of the vibrational mode associated with the dissociation (Fe-CO stretch) is 480 cm⁻¹ as calculated by the B3LYP functional. This translates to about 70 fs period time. This correlates well with the observed time scale of the photodissociation process of 50 fs³³ and suggests that the dissociation occurs within one vibrational period.

Summary and Conclusions

In this work, we have investigated the initial steps of the photodissociation process of CO-ligated heme by means of time-dependent density functional theory. For this objective, we have calculated the excited states of heme-CO along the iron-CO

stretch coordinate without relaxation of the other nuclear degrees of freedom. Our results show that the 3 A' and 5 A'' states are repulsive along the iron-CO stretch coordinate and cross the energetically lowest and initially excited Q states (1 A' and 1 A'') of heme-CO at an Fe-CO distance of 2 Å. From this distance on, the repulsive states are the energetically lowest singlet states of the system.

Our results help to resolve the initial steps of the CO ligated heme photodissociation process. Upon excitation of heme-CO into the Q states, it decays nonradiatively into the dissociative states (identified as 3 A' and 5 A'' at equilibrium structure). The analysis of these states at the ground-state equilibrium geometry has been performed using attachment/detachment density plots. At the ground-state equilibrium geometry, the repulsive states correspond to excitations from a binding combination of an iron d orbital and the π^* orbital of CO (the so-called back-bonding) to an antibonding combination (anti-back-bonding). At a separation of 2.5 Å, the excited states have already substantial iron-to-ligand charge-transfer character. These results are supported by the previous experimental assignment of the first intermediate to be a iron-to-ring charge-transfer state.³³ Further decay and recovery of the ground state of unligated heme, which is accompanied by a change in spin state, has to evolve from these repulsive states.

In the future, we plan to investigate the triplet ground and excited states of CO ligated and unligated heme to give the remaining pieces of the puzzle of the complete dissociation process. Preliminary calculations indicate that one or two additional intermediate triplet states are involved before the high-spin ground state of unligated heme is reached. As noted, geometry relaxation seems not to play a major role in the photodissociation process of CO ligated heme. Thus, the photodissociation can be treated as a local perturbation to the full proteins Mb and Hb which are used in the experiments. This on the other hand justifies the use and clarifies the success of small model complexes to simulate and reproduce experimental data obtained with the complete proteins.

Acknowledgment. A.D. gratefully acknowledges financial support by the Deutsche Forschungsgemeinschaft as an "Emmy-Noether" fellow. This work was supported by the Director, Office of Energy Research, Office of Basic Energy Sciences, Chemical Sciences Division of the U.S. Department of Energy under Contract No. DE-AC03-76SF00098. M.H.-G. is on an appointment as a Miller Research Professor in the Miller Institute for Basic Research in Science.

References and Notes

- (1) Nienhaus, G. U.; Mourant, J. R.; Frauenfelder, H. *Proc. Natl. Acad. Sci. U.S.A.* **1992**, *89*, 2902.
- (2) Frauenfelder, H.; McMahon, B. H.; Austin, R. B.; Chu, K.; Groves, J. T. *Proc. Natl. Acad. Sci. U.S.A.* **2001**, *98*, 2370.
- (3) Campbell, B. F.; Chance, M. R.; Friedman, J. M. *Science* **1987**, *238*, 373.
- (4) Huang, J.; Ridsdale, A.; Wang, J.; Friedman, J. M. *Biochemistry* **1997**, *36*, 14353.
- (5) Nienhaus, G. U.; Mourant, J. R.; Chu, K.; Frauenfelder, H. *Biochemistry* **1994**, *33*, 13413.
- (6) Nienhaus, K.; Lamb, D. C.; Pengchi, D.; Nienhaus, G. U. *Biophys. J.* **2002**, *82*, 1059.
- (7) Pauling, L.; Coryell, C. D. *Proc. Natl. Acad. Sci. U.S.A.* **1936**, *22*, 210.
- (8) Stec, B.; Phillips, G. N., Jr. *Acta Crystallogr.* **2001**, *D54*, 751.
- (9) Kachalova, G. S.; Pepov, A. N.; Bartunik, H. D. *Science* **1999**, *284*, 473.
- (10) Vojtechovsky, J.; Schlichting, I.; Chu, K.; Sweet, R. M.; Berendzen, J. *Biophys. J.* **1999**, *77*, 2153.
- (11) St. George, R. C.; Pauling, L. *Science* **1951**, *114*, 629.
- (12) Pauling, L.; Weiss, J. J. *Nature* **1964**, *203*, 182.

- (13) McMahon, M. T.; deBios, A. C.; Godbout, N.; Salzman, R.; Laws, D. D.; Hongbiao, L.; Havlin, R. H.; Oldfield, E. *J. Am. Chem. Soc.* **1998**, *120*, 4784.
- (14) Suematsu, M.; Wakabayashi, Y.; Ishimura, Y. *Cardiovas. Res.* **1996**, *32*, 679.
- (15) Møller, J. K. S.; Skibsted, L. H. *Chem. Rev.* **2002**, *102*, 1167–1178.
- (16) Mizutani, Y.; Kitagawa, T. *J. Phys. Chem. B* **2001**, *105*, 10992.
- (17) Jackson, T. A.; Lim, M.; Anfinrud, P. A. *Chem. Phys.* **1994**, *180*, 131.
- (18) Bendall, D. S. *Protein Electron Transfer*, BIOS Scientific: Oxford, 1996.
- (19) Bellelli, A.; Brunori, M.; Brezezinski, P.; Wilson, M. T. *Methods* **2001**, *24*, 139.
- (20) Spiro, T. G.; Kozlowski, P. M. *J. Am. Chem. Soc.* **1998**, *120*, 4524.
- (21) Service, R. F. *Science* **1995**, *269*, 921.
- (22) Norvell, J. C.; Nunes, A. C.; Schoenborn, B. P. *Science* **1975**, *190*, 568.
- (23) Kuriyan, J.; Wilz, S.; Karplus, M.; Petsko, G. A. *J. Mol. Biol.* **1986**, *192*, 133.
- (24) Quillin, M. L.; Arduini, R. M.; Olson, J. S.; Phillips, G. N. J. *J. Mol. Biol.* **1993**, *234*, 140.
- (25) Yang, F.; Phillips, G. N. J. *J. Mol. Biol.* **1996**, *256*, 762.
- (26) Ray, G. B.; Li, X.-Y.; Ibres, J. A.; Sessler, J. L.; Spiro, T. G. *J. Am. Chem. Soc.* **1994**, *116*, 162.
- (27) Ivanov, D.; Sage, J. T.; Keim, M.; Powell, J. R.; Asher, S. A.; Champion, P. M. *J. Am. Chem. Soc.* **1994**, *116*, 4139.
- (28) Lim, M.; Jackson, T. A.; Anfinrud, P. A. *Science* **1995**, *269*, 962.
- (29) Brunori, M.; Giacometti, G. M.; Antonini, E.; Wyman, J. *Proc. Natl. Acad. Sci. U.S.A.* **1973**, *70*, 3141.
- (30) Antonini, E.; Brunori, M. *Hemoglobin and Myoglobin in their reaction with Ligands*; North-Holland: Amsterdam, 1971.
- (31) Greene, B. I.; Hochstrasser, R. M.; Weisman, R. B.; Eaton, W. A. *Proc. Natl. Acad. Sci. USA* **1978**, *75*, 5255.
- (32) Petrich, J. W.; Poyart, C.; Martin, J. L. *Biochemistry* **1988**, *27*, 4049.
- (33) Franzen, S.; Kiger, L.; Poyart, C.; Martin, J.-L. *Biophys. J.* **2001**, *80*, 2372.
- (34) Waleh, A.; Loew, G. H. *J. Am. Chem. Soc.* **1982**, *104*, 2346.
- (35) Zerner, M.; Gouterman, M.; Kobayashi, H. *Theo. Chim. Acta* **1966**, *6*, 3831.
- (36) Vogler, A.; Kunkely, H. *Ber. Bunsen-Ges. Phys. Chem.* **1976**, *80*, 425.
- (37) Tokita, Y.; Nakatsuji, H. *J. Phys. Chem. B* **1997**, *101*, 3281–3289.
- (38) McMahon, B. H.; Stojkovic, B. P.; Hay, P. J.; Martin, R. L.; Garcia, A. E. *J. Chem. Phys.* **2000**, *113* (16), 6831–6850.
- (39) Derewenda, Z.; Dodson, G.; Emsley, P.; Harris, D.; Nagai, K.; Perutz, M.; Reynaud, J.-P. *J. Mol. Biol.* **1990**, *211*, 515.
- (40) Della Longa, S.; Arcovito, A.; Girasole, M.; Hazemann, J. L.; Benfatto, M. *Phys. Rev. Lett.* **2001**, *87*, 155501.
- (41) Mäkinen, M. W.; Eaton, W. *Ann. N.Y. Acad. Sci.* **1973**, *206*, 210.
- (42) Hay, P. J.; Wadt, W. R. *J. Chem. Phys.* **1985**, *82*, 299.
- (43) Head-Gordon, M.; Grana, A. M.; Maurice, D.; White, C. A. *J. Phys. Chem.* **1995**, *99*, 14261.
- (44) Kong, J.; White, C. A.; Krylov, A. I.; Sherrill, D.; Adamson, R. D.; Furlani, T. R.; Lee, M. S.; Lee, A. M.; Gwaltney, S. R.; Adams, T. R.; Ochsenfeld, C.; Gilbert, A. T. B.; Kedziora, G. S.; Rassolov, V. A.; Maurice, D. R.; Nair, N.; Shao, Y.; Besley, N. A.; Maslen, P. E.; Dombroski, J. P.; Daschel, H.; Zhang, W.; Korambath, P. P.; Baker, J.; Byrd, E. F. C.; Van Voorhis, T.; Oumi, M.; Hirata, S.; Hsu, C.-P.; Ishikawa, N.; Florian, J.; Warshel, A.; Johnson, B. G.; Gill, P. M. W.; Head-Gordon, M.; Pople, J. A. *J. Comput. Chem.* **2000**, *21* (16), 1532–1548.
- (45) Kozlowski, P. M.; Spiro, T. G.; Berces, A.; Zgierski, M. Z. *J. Phys. Chem. B* **1998**, *102*, 2603.
- (46) Hartmann, H.; Zinser, S.; Komninos, P.; Schneider, R. T.; Nienhaus, G. U.; Parak, F. *Proc. Natl. Acad. Sci. U.S.A.* **1996**, *93*, 7013.
- (47) Dreuw, A.; Dunietz, B. D.; Head-Gordon, M. *J. Am. Chem. Soc.* **2002**, *124* (41), 12070.